Non-Gaussian beam dynamics in low energy antiproton storage rings

J. Resta-López[a], J. R. Hunt[a], C. P. Welsch[a]

[a] *The Cockcroft Institute, University of Liverpool, United Kingdom*

Abstract

In low energy antiproton facilities, where electron cooling is fundamental, the cooling forces together with heating phenomena causing emittance blow-up, such as Intra Beam Scattering (IBS), result in highly non-Gaussian beam distributions. In these cases, a precise simulation of IBS effects is essential to realistically evaluate the long term beam evolution, taking into account the non-Gaussian characteristics of the beam. Here, we analyse the beam dynamics in the Extra Low ENergy Antiproton ring (ELENA), which is a new small synchrotron currently being constructed at CERN to decelerate antiprotons to energies as low as 100 keV. Simulations are performed using the code BETA-COOL, comparing different models of IBS.

Keywords: Beam dynamics; Low energy storage rings; Antiprotons; Intra-beam scattering; Numerical simulations

1. Introduction

Antiprotons, stored and cooled at low energies in a storage ring or at rest in traps, are highly desirable for the investigation of a large number of basic questions on fundamental interactions, on the static structure of exotic antiprotonic atomic systems or of (radioactive) nuclei as well as on the time-dependent quantum dynamics of correlated systems. The Antiproton Decelerator (AD) at CERN [1] is currently the world's only low energy antiproton factory dedicated to antimatter experiments. The development of new antiproton facilities, such as the Extremely Low ENergy Antiproton ring (ELENA) [2] to further decelerate

Email address: jrestalo@liverpool.ac.uk (J. Resta-López)

beams from the AD in a well controlled manner, will open a unique possibility to provide cooled, high-quality beams of extra-low energy antiprotons.

ELENA is a small synchrotron equipped with an electron cooler, which is currently being constructed at CERN to further decelerate antiprotons from the AD from 5.3 MeV to kinetic energies as low as 100 keV with a beam population of $\sim 10^7$ cooled antiprotons. At such low energies it is very important to carefully take contributions from electron cooling (e-cooling) and heating effects into account. Among these heating effects is Intra-Beam Scattering (IBS), which is one of the main limiting processes for the performance of typical low energy ion storage rings.

For simplicity, initial Gaussian beam distributions are usually assumed for beam dynamics simulations in low energy ion rings. For instance, for ELENA beam dynamics simulations of the cooling process in presence of rest gas scattering and IBS have been done in [3, 4]. In both cases, initial Gaussian antiproton beam distributions were assumed and a standard IBS model (the so-called Martini model [5]) was used. In [3, 4] simulations led to an overcooling of the beam core and highly populated long amplitude tails. We suspect that this overcooling result is unphysical and an artefact of considering standard IBS models.

Standard algorithms to estimate IBS are based on the growth of the rms parameters of Gaussian distributions [5–8] and, thus, allow long term evolutions of emittances only if the beam remains Gaussian. However, in many of these facilities, where electron cooling is a fundamental part, the cooling forces result in highly non-Gaussian beam distributions. In these cases, other algorithms applicable for a non-Gaussian distribution of IBS effects are required to realistically evaluate the long term beam evolution.

To address this matter we have investigated the e-cooling process in ELENA by means of beam dynamics simulations using the code BETACOOL [9] and comparing different models of IBS for the first cooling plateau at the intermediate beam momentum 35 MeV/c. A particularity of these studies is the use of input beam distributions based on real measurements of beam profiles in the AD. Our final goal is to make a more precise description of the beam evolution during the cooling process under more realistic assumptions.

2. ELENA cycle

In ELENA electron cooling will be used to counteract the emittance and the relative momentum spread blow-up caused by the deceleration process. This will increase the efficiency of typical experiments capturing the antiprotons in traps by one to two orders of magnitude.

The ELENA deceleration cycle is schematically shown in Fig. 1. There are two cooling plateaus: the first cooling plateau lasts approximately 8 s at 35 MeV/c momentum, and the second one is applied for 2 s at 13.7 MeV/c. In both cases the cooling is applied to a coasting beam. A third cooling at 13.7 MeV/c will be applied to bunched beams prior to extraction.

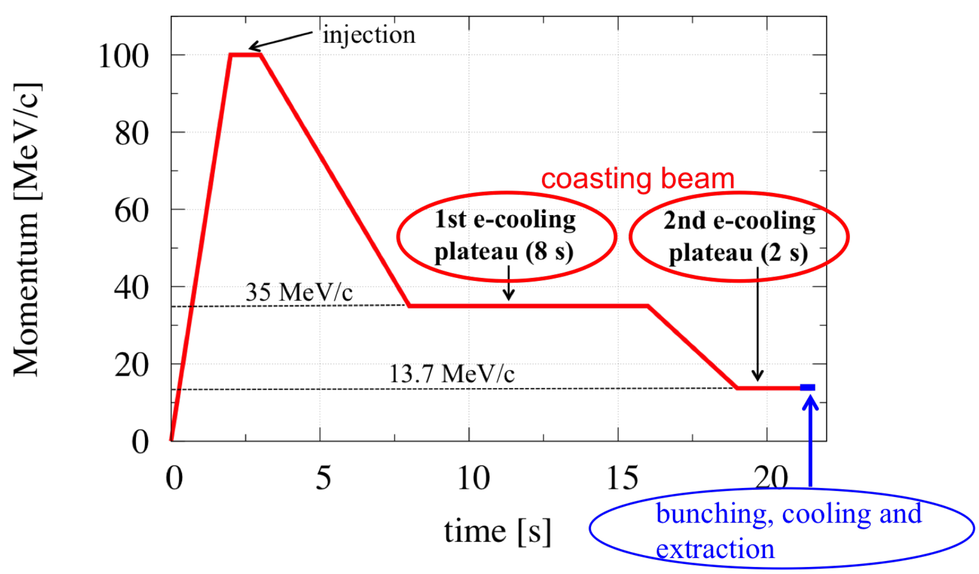

Figure 1: Basic ELENA deceleration cycle.

The ELENA optics layout, matched using the accelerator design code MAD-X [10], is depicted in Fig. 2 and is described in detail in [2, 11]. In Table 1 we display some relevant nominal parameters.

Table 1: ELENA nominal machine and beam parameters.

Circumference (m)	30.4
Nominal (dynamic) vacuum pressure (Torr)	3×10^{-12}
Machine tunes Q_x/Q_y	2.3/1.3
Repetition rate (s)	≈ 100
Kinetic energy range (MeV)	5.3 – 0.1
Momentum range (MeV/c)	100 – 13.7
Beam intensity (number of $\bar{\mathrm{p}}$)	$\sim (1-3)\times 10^7$
Transverse acceptance (μm)	75
Ejected emittance (rms) $\epsilon_{x,y}$ (π mm mrad)	~ 1
Ejected relative momentum spread (rms) σ_p/p (%)	~ 0.05
Number of ejected bunches	4
Ejected bunch length (m)	1.3

3. Beam distribution at injection

Beam profile measurements in the AD in the past [12] have shown non-Gaussian transverse beam distributions with compact core and extended tails, generated during the beam cooling process (stochastic cooling and e-cooling). Figure 3 shows an example of beam distribution measurements performed by scraping in the AD at 100 MeV/c momentum. A scraper blade, located in a position with zero dispersion, has been moved into the beam in small steps to measure the remaining beam current. This allows us to obtain cumulative distribution functions. The differentiation of these cumulative functions corresponds to the density of the beam distribution. Actually, the measurement in Fig. 3 represents half of the beam distribution. For this set of measurements approximate physical rms emittances of $\epsilon_x = 0.2$ to 0.5 μm were inferred for the horizontal phase space, and $\epsilon_y = 0.15$ to 0.3 μm for the vertical phase space.

In recent years, such a core-tail beam structure in the AD has been confirmed using Gas Electron Multiplier (GEM) based beam profile monitors [13, 14].

For the beam dynamics simulations in ELENA we use measured parameters

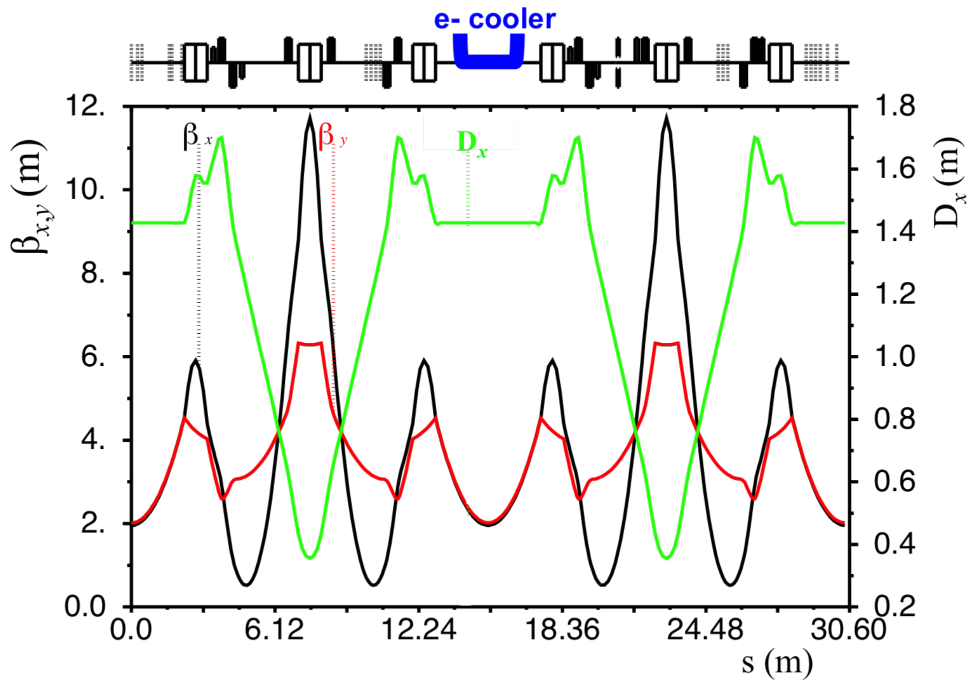

Figure 2: ELENA ring optics.

in the AD as a reference to generate an input distribution of macro-particles to be injected into the ELENA ring. For it, a Python script is used to create an input core-tail distribution based in the sum of two Gaussian functions in phase space centered at zero mean values:

$$g(x,x') = N\left\{(1-w)\frac{1}{2\pi\epsilon_{\rm c}}\exp\left[-\frac{I(x,x')}{2\epsilon_{\rm c}}\right] + w\frac{1}{2\pi\epsilon_{\rm t}}\exp\left[-\frac{I(x,x')}{2\epsilon_{\rm t}}\right]\right\}, \quad (1)$$

where $\epsilon_{\rm c}$ stands for the core emittance and $\epsilon_{\rm t}$ for the emittance of the Gaussian phase space representing the tails; N is the total number of macro-particles, and the parameter w represents a relative weight. The term $I(x,x')$ is the so-called Courant-Snyder invariant,

$$I(x,x') = \gamma_x x^2 + 2\alpha_x x x' + \beta_x x'^2, \quad (2)$$

with β_x, α_x and $\gamma_x \equiv (1+\alpha_x^2)/\beta_x$ the Courant-Snyder parameters.

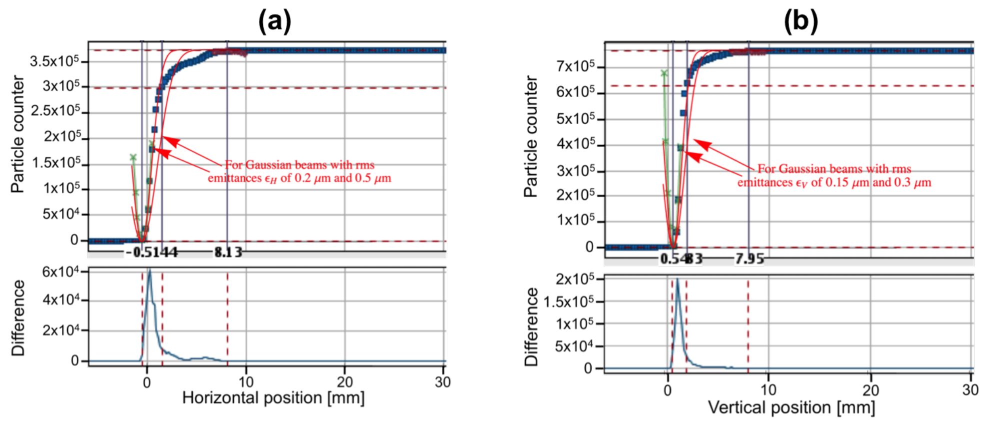

Figure 3: Horizontal (a) and vertical (b) half beam profile measured using a scraper in the AD at 100 MeV/c, taken in 2011. Courtesy of T. Eriksson.

Here, the emittance can be given in terms of the standard deviation $\sigma_{\mathrm{c,t}}$ for the betatronic beam width for the core and the tail, respectively, and the optics parameter β_x: $\epsilon_{\mathrm{c,t}} = \sigma^2_{\mathrm{c,t}}/\beta_x$.

A similar distribution $g(y, y')$ is assumed for the vertical phase space, with the corresponding optics parameters β_y, α_y and γ_y.

A Gaussian longitudinal phase space is considered for injection from AD to ELENA. Figure 4 shows a typical longitudinal profile measurement using tomography techniques in the AD [15]. In this sample the following parameters were measured: rms bunch length $\sigma_\tau = 125$ ns; rms kinetic energy spread $\sigma_E = 4$ keV; and relative rms momentum spread $\sigma_p/p = (1/2)\sigma_E/E_0 = 0.38 \times 10^{-3}$ (with the nominal energy $E_0 = 5.3$ MeV at the end of the AD cycle).

Figure 5 depicts the initial distribution of macroparticles at injection used for the particle tracking simulations in ELENA, based on the above assumptions. The following conservative values have been taken into account:

- For the transverse phase space, based on Eq. (1), we use the following emittance values: $(\epsilon_c)_{\mathrm{inj}} = 0.5$ μm, and the tail is extended to $3\times(\sigma_t)_{\mathrm{inj}} \approx 10$ mm, for both vertical and horizontal planes. For simplicity, here the same number of macroparticles in the core and in the tail is assumed, i.e.

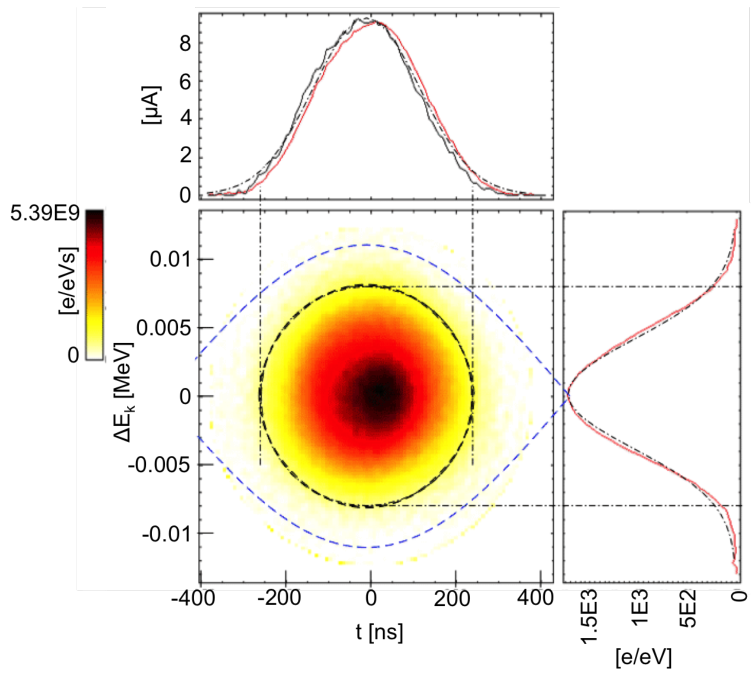

Figure 4: Longitudinal beam profile (kinetic energy spread versus time structure) measurement in the AD at 100 MeV/c, taken in 2011. Courtesy of T. Eriksson.

$w = 0.5$.

- For the longitudinal phase space, the ELENA bunch must be scaled by a factor 0.8 from the AD bunch. For example, scaling from the bunch in Fig. 4 one finds $(\sigma_\tau)_{\rm inj} \approx 100$ ns rms bunch length (in units of time) and $(\sigma_p/p)_{\rm inj} \approx 0.3 \times 10^{-3}$ for the relative rms momentum spread.

4. Beam dynamics simulations

After injection from the AD to ELENA, the beam is decelerated for 5 s from a momentum of 100 MeV/c down to an intermediate momentum of 35 MeV/c. Assuming deceleration with constant RF voltage[1], the physical emittances of

[1]For simplicity, we have assumed no increase of RF voltage for beam transfer from injection to the start of the first deceleration ramp, and, therefore, no variation of relative

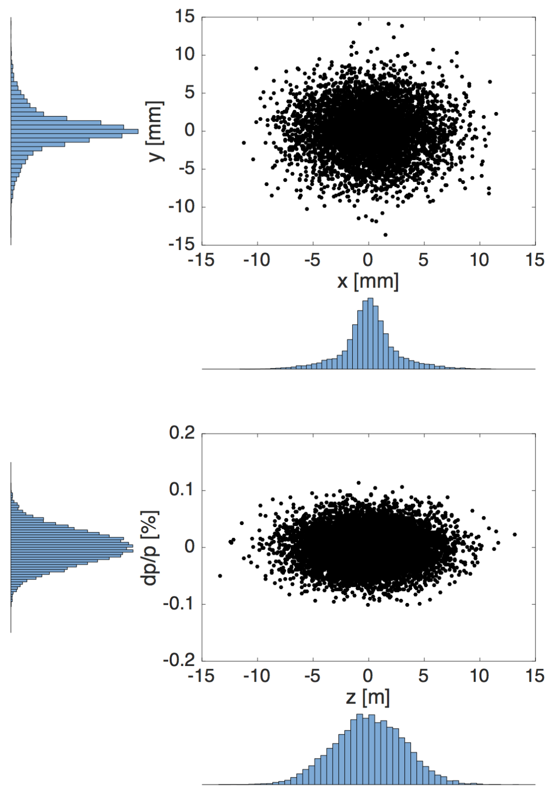

Figure 5: Transverse (top) and longitudinal (bottom) beam profile injected from the AD to ELENA at 100 MeV/c momentum. Distribution of 10000 macroparticles.

the beam and the relative momentum spread increase adiabatically by a factor $f_{\mathrm{a}} = (\beta\gamma)_1/(\beta\gamma)_2 \simeq 2.86$, where β_1 refers to the relativistic velocity factor at the beginning ($p = 100$ MeV/c) and β_2 at the end ($p = 35$ MeV/c) of the deceleration ramp, respectively; γ is the corresponding Lorentz factor ($\gamma \approx 1$ at low energies).

Then, the antiproton beam is iso-adiabatically debunched prior to electron cooling. This debunching process implies a blow-up by approximately a factor

momentum spread at this stage. A more detailed description of the different scenarios of the RF gymnastics for ELENA can be found in [2].

$\pi/2$ for the longitudinal emittance [16], and a momentum spread reduction [2] by a factor:

$$f_{\text{iso}} = \frac{\pi^2}{2}\sqrt{\frac{\pi}{2}}\frac{(\sigma_\tau)_\text{b}}{T_\text{rev}} \simeq 0.65, \tag{3}$$

where $(\sigma_\tau)_\text{b} = f_\text{a} \cdot (\sigma_\tau)_\text{inj} \simeq 286$ ns is the bunch length (in units of time) before debunching.

Then, e-cooling is applied for 8 s (first cooling plateau, see Fig. 1) to the coasting antiproton beam. Figure 6 shows a distribution of 10^4 macroparticles at the beginning of the e-cooling process at 35 MeV/c. The beam dimensions of this distribution are given by: $f_\text{a}^{1/2} \cdot (\sigma_c)_\text{inj} \simeq 1.73$ mm, $f_\text{a}^{1/2} \cdot (\sigma_t)_\text{inj} \simeq 5.64$ mm, and $f_\text{iso} \cdot f_\text{a} \cdot (\sigma_p/p)_\text{inj} \simeq 0.56 \times 10^{-3}$, where the blow-up scaling factors f_a and f_iso are taken into account as described before with respect to the values at injection. This ensemble of macroparticles is used as an input for the code BETACOOL [9]. This code allows us to calculate the evolution of arbitrary beam distributions under the action of cooling forces and different scattering effects, such as rest gas scattering and IBS. The code BETACOOL has been benchmarked with measurements in the past, for example in the context of the low energy ion ring ELISA [17], giving a reasonable agreement.

4.1. Electron cooling

The electron cooling is a well consolidated technique to obtain high-quality ion beams by means of increasing the 6D phase space density through the dissipative force created by Coulomb interaction of the beam particles with a lower temperature electron distribution [18].

The electron cooling systems employed at low-energy coolers are typically based on an electron beam immersed in the longitudinal magnetic field of a

[2] The corresponding momentum spread reduction due to bunching/debunching can be calculated using the typical longitudinal emittance definitions: $\epsilon_L = 4\pi\beta c\sigma_p\sigma_\tau$ for bunched beam and $\epsilon_L = 4(2/\pi)^{1/2}\beta c\sigma_p T_\text{rev}$ for coasting beam, where $T_\text{rev} = C/(\beta c)$ is the beam time revolution, with C the ring circumference.

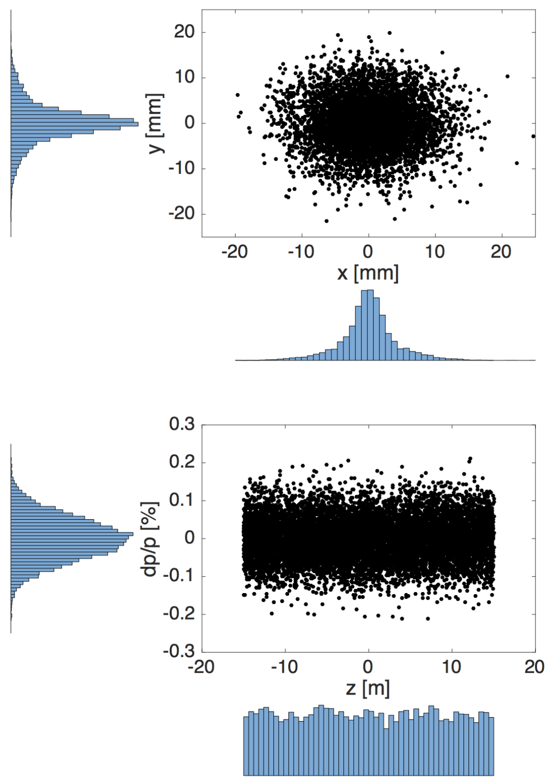

Figure 6: Transverse (top) and longitudinal (bottom) beam profile at the beginning of the first e-cooling plateau at 35 MeV/c momentum. Distribution of 10000 macroparticles.

solenoid (magnetised electron beam). For magnetised electron distributions, several theoretical models for the e-cooling friction force have been proposed in the literature, see e.g. [19–22]. A comparison of different electron cooling models is outside the scope of this paper. An exhaustive analysis of the different models, their validity ranges and limitations, can be found in [23]. Here, for the ELENA e-cooler simulations, to account for the finite value of the magnetic solenoidal field, we have used the so-called Parkhomchuk empirical expression [22]:

$$\vec{F} = -\vec{V}\frac{4Z^2e^4n_e}{m_e}\frac{L_M}{\left(V^2+\Delta_{e,\mathrm{eff}}^2\right)^{3/2}}, \tag{4}$$

where Z is the ion charge number, e is the electron charge, n_e is the electron density, m_e is the electron mass, $\vec{V}$ is the relative ion velocity, $\Delta_{e,\mathrm{eff}}$ is the effective velocity spread of the electrons, and L_M is the Coulomb logarithm, which is defined as:

$$L_M = \ln\left(\frac{\rho_{\max} + \rho_{\min} + \rho_L}{\rho_{\min} + \rho_L}\right), \tag{5}$$

with $\rho_{\max}$ and $\rho_{\min}$ the maximum and minimum impact parameters, respectively; $\rho_L = m_e c \Delta_{e,\perp}/(eB)$. For ELENA we can approximate $L_M \cong 10$.

The expression (4) has been benchmarked with measurements [24], showing a reasonable agreement, and it seems sufficiently accurate to be used for a simple estimate of the e-cooler performance. Among others, Eq. (4) is implemented in the BETACOOL code.

Here, we consider a cylindrical uniform electron beam distribution with transverse temperature $k_B T_{e\perp} = 0.01$ eV and longitudinal temperature $k_B T_{e\parallel} = 0.001$ eV (with k_B the Boltzmann constant). The space charge in the e-beam is also taken into account. It generates a parabolic distribution of e-beam velocities. Relevant parameters of the ELENA e-cooler are summarised in Table 2. A complete description of the ELENA e-cooler can be found in [2, 3].

4.2. Intra-beam scattering

IBS is one of the main heating processes limiting the performance of low energy ion rings. It becomes especially stronger when the phase space volume of the beam is reduced by cooling, thus limiting the achievable final emittances, which are determined by an equilibrium state between IBS and cooling.

IBS is a beam heating effect produced by multiple small-angle Coulomb scattering of charged particles within the beam itself. It causes an exchange of energy between the transverse and longitudinal degrees of freedom, thus leading to the growth of the phase space area occupied by the beam.

Many of the theories of IBS extensively described in the literature, e.g. [5–8], and frequently used in simulations to calculate the IBS growth rates and its effect on the beam are only valid for Gaussian distributions, which is unlikely

Table 2: ELENA electron cooler parameters

Beam momentum [MeV/c]	35 – 13.7
Velocity factor, $\beta = v/c$	0.037 – 0.015
Electron beam energy [eV]	355 – 55
Electron current, I_e [mA]	5 – 2
Electron beam density, n_e [10^{12} m^{-3}]	1.38 – 1.41
Magnetic field in the gun, B_{gun} [G]	1000
Magnetic field in the drift, B_{drift} [G]	100
Expansion factor	10
Cathode radius [mm]	8
Electron beam radius, r_b [mm]	25
Betatron functions, $\beta_{x,y}$ [m]	2.103, 2.186
Horizontal dispersion, $D_x[m]$	1.498
Flange-to-flange length [m]	1.93
Solenoid length [m]	1.0
Effective length (good field region) [m]	0.7
Electron beam transverse temperature, $k_B T_{e\perp}$ [eV]	0.01
Electron beam longitudinal temperature, $k_B T_{e\parallel}$ [eV]	0.001

in many cases. For instance, during the e-cooling process the beam distribution can quickly deviate from a Gaussian, resulting in a very dense core with long tails. In addition, the injected beam from a previous machine of the decelerator chain may be highly non-Gaussian, as likely the beam injected from the AD to ELENA will be.

In ELENA, previous simulations of the cooling process, assuming an input Gaussian beam and using a standard IBS model (the Martini model [5]) pointed out an overcooling of the core and highly populated long tails [3, 4]. This core overcooling looks unphysical and a product of a simulation artefact due to the assumption of the Gaussian approximation.

Although the Gaussian approximation is still useful for a relative analysis, for a more realistic estimate of the beam evolution it would be more correct to pay attention to the non-Gaussian structure of the beam. In this case, it is necessary to apply IBS induced kicks based on diffusion coefficients which are different for particles inside and outside of the core.

Different IBS models for non-Gaussian distributions have been proposed in the literature [25–30], and implemented in the code BETACOOL [31]. A preliminary study of the intra-beam scattering effects in ELENA using a core-tail model was presented in [32].

Here, we compare results using the following IBS models:

- Standard model: here, we use the so-called Martini model [5]. This model is an extended version of Piwinski's model [6], taking into account lattice derivatives. The computation process can basically be summarised as follows: rms emittances and momentum spread are computed from the input macro-particle distribution; the growth rates are calculated at each element of the lattice along the ring, assuming Gaussian beams with these rms parameters; and, finally, random IBS kicks are then applied to the full macro-particle distribution based on the calculated growth rates.

- Simplified kinetic model: based on the three-dimensional approximate algorithm described in [29]. This model is based on a numerical solution of the Fokker-Planck equation, assuming the following approximations: (1) the friction force has a linear dependence on momentum; (2) the components of the diffusion tensor are constant. The components of the diffusion tensor are calculated in accordance with the Bjorken-Mtingwa formulae [7]. This model also assumes that most of the IBS interactions take place inside the beam core, which is usually close to a Gaussian distribution.

- Local model [30]: this algorithm takes into account the local density of particles after establishing an array of particles in the total beam distribution. It calculates the diffusion tensor components locally through the Coulomb scattering of a test particle with the nearest particles. The diffusion components are calculated at each optical element of the ring. This algorithm can be applied to any arbitrary particle distribution and is very suitable to precisely describe IBS effects during cooling processes in hadron storage rings. However, this algorithm requires much longer computation times than the previous models.

4.3. Beam evolution

Figure 7 illustrates our beam dynamics simulation sequence. A distribution of 10^4 macro-particles is tracked through the ELENA lattice using the model beam algorithm of BETACOOL to study the beam evolution with e-cooling at 35 MeV/c $\bar{\mathrm{p}}$ momentum. For this study the initial beam structure is shown in Fig. 6, based on the bi-Gaussian function of Eq. (1) and applying the corresponding scaling factors, as described in previous sections. The optics lattice information is generated by the code MAD-X [10] and read by BETACOOL.

The beam is cooled down for 8 s by e-cooling. In addition, IBS is switched on. In these simulations we have also taken into account the effect of rest gas scattering, considering the nominal vacuum pressure $P = 3 \times 10^{-12}$ Torr, and the following outgassing species: 95% H_2, 2% CO, 2% CO_2 and 1% CH_4 with a total gas density (at room temperature) of 9.6×10^{10} m^{-3} [33]. Although included in these simulations for the sake of completeness, for ELENA with the

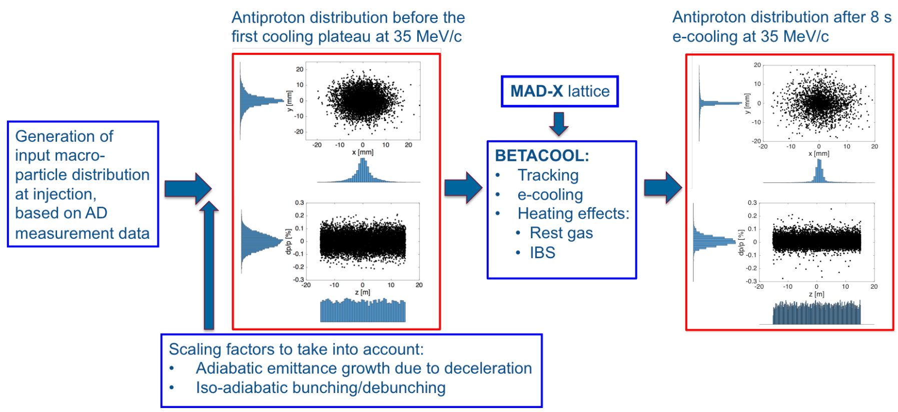

Figure 7: Schematic description of the simulation sequence of the Monte Carlo multiparticle tracking in the ELENA ring applying e-cooling and different heating scattering effects. The transverse and longitudinal beam profiles at the beginning of the first e-cooling plateau at 35 MeV/c momentum are shown on the left hand side. The resulting beam profiles after 8 s e-cooling are shown on the right hand side.

nominal vacuum pressure of 3×10^{-12} Torr, the effect of rest gas scattering has been estimated to be practically negligible in comparison with IBS [4, 34].

In principle, a local IBS model will allow us to make a self-consistent estimate of the beam evolution. In these simulations the integration time step is 0.5 s. To apply the IBS effect locally we have established cells with dimensions of 0.1σ and 100 local particles each. For the IBS simulations the friction and diffusion coefficients are calculated at each optical element of the lattice.

The rms emittance and momentum spread evolution is shown in Fig. 8, where the e-cooling process is compared in presence of three different IBS models: local, kinetic and standard IBS (see Sec. 4.2 for details). One can see that applying a local IBS model results in slightly higher rms emittances. On the other hand, for the cases of the kinetic and the standard IBS models, the results are practically similar.

In Fig. 8 there is also an interesting feature of the evolution of the relative rms momentum spread (σ_p/p) for the case of e-cooling plus the local IBS model. Around 5 s there is a sudden increase of σ_p/p (rms). If we looked at the scatter plots of the transverse and longitudinal beam profiles after 8 s cooling (Fig. 9), one can see that a few macroparticles have been kicked to high momentum spread, $|\Delta p/p| > 0.5\%$. In the transverse plane, some macroparticles can even be scattered outside the effective physical aperture of the machine (60 mm diameter), and get lost. Of course, these few macroparticles at high amplitude increase significantly the rms parameters of the distribution.

The emittance as a rms quantity is biased by strong tails. Therefore, in order to calculate the rms parameters concentrating the relevant part of the distribution, cuts on the final distribution must be applied. In this case, we can establish the following amplitude cuts: -30 mm $< x, y <$ 30 mm and $-0.5\% < \Delta p/p < 0.5\%$. Alternatively, we can use the emittance definition according to the value that encompasses a specific percentage of the beam. For example, to follow just the evolution of the dense core we could calculate the emittance within 68% of the distribution and, to extend the study to the core-tail evolution, we could evaluate the beam invariants within 95% of the distribution. Figure 10 shows the evolution of the transverse emittances and relative momentum spread for half bem widths containing 68% and 95% of the particles, respectively.

After 8 s cooling, $\epsilon_{x,y}$ (68%) and σ_p/p (68%) approach to equilibrium values, while $\epsilon_{x,y}$ (95%) monotonically decreases far from achieving equilibrium values. The narrow core (68%) will reach a cooling-IBS equilibrium faster than the high amplitude tails (within 95%), which will require much longer time.

Table 3 summarises the emittances and relative momentum spread values for the ELENA first cooling plateau for the different algorithms studied.

The beam profiles at the end of the cooling process for 35 MeV/c beam momentum are shown in Fig. 11, comparing the results for the three IBS models under study. On the one hand, the cooling of the core is smoother if an IBS local model is applied and, likely, it describes more accurately the actual process, since it is beam shape-independent. On the other hand, applying the standard model and the simplified kinetic model results in an overcooling of the beam core.

Table 3: Emittance and relative momentum spread before and after 8 s e-cooling at the intermediate (35 MeV/c) plateau of the ELENA cycle. The rms values and values based on the enclosed particles within 68% and 95% of the antiproton distribution are shown for simulations using different algorithms of IBS.

Beginning first cooling plateau	
ϵ_x / ϵ_y (rms) [π mm mrad]	8.4 / 8.23
σ_p/p (rms)	0.56×10^{-3}
ϵ_x / ϵ_y (68%) [π mm mrad]	14.09 / 13.67
σ_p/p (68%)	0.56×10^{-3}
ϵ_x / ϵ_y (95%) [π mm mrad]	71.21 / 69.82
σ_p/p (95%)	1.1×10^{-3}
After 8 s e-cooling + Standard IBS	
ϵ_x / ϵ_y (rms) [π mm mrad]	3.28 / 3.2
σ_p/p (rms)	0.25×10^{-3}
ϵ_x / ϵ_y (68%) [π mm mrad]	0.08 / 0.076
σ_p/p (68%)	9.92×10^{-5}
ϵ_x / ϵ_y (95%) [π mm mrad]	43.72 / 42.57
σ_p/p (95%)	0.67×10^{-3}
After 8 s e-cooling + Kinetic IBS	
ϵ_x / ϵ_y (rms) [π mm mrad]	3.29 / 3.28
σ_p/p (rms)	0.24×10^{-3}
ϵ_x / ϵ_y (68%) [π mm mrad]	0.12 / 0.57
σ_p/p (68%)	8.73×10^{-5}
ϵ_x / ϵ_y (95%) [π mm mrad]	44.64 / 42.44
σ_p/p (95%)	0.64×10^{-3}
After 8 s e-cooling + Local IBS	
ϵ_x / ϵ_y (rms) [π mm mrad]	3.45 / 3.4
σ_p/p (rms)	0.39×10^{-3}
ϵ_x / ϵ_y (68%) [π mm mrad]	1.55 / 1.34
σ_p/p (68%)	0.34×10^{-3}
ϵ_x / ϵ_y (95%) [π mm mrad]	46.3 / 43.83
σ_p/p (95%)	0.73×10^{-3}

Moreover, in Fig. 11 the momentum spread profile presents an interesting asymmetry. It presents a longer tail for positive $\Delta p/p$ values, likely caused by a slight acceleration of antiprotons in the tails due to e-beam (from the cooler) space charge effects. This point requires further investigation.

5. Conclusions and prospects

The AD-ELENA complex at CERN will provide cooled, high quality beams of 100 keV kinetic energy antiprotons at intensities exceeding those achieved presently at the AD by a factor of ten to one hundred. This will improve by the same factor the efficiency of antihydrogen production, opening the door to unique antimatter experiments.

In order to design and optimise such machines it is important to accurately simulate the beam evolution performance. It will allow us to predict the quality of the beam and its evolution at the different stages of the machine cycle. The main limiting effect during the beam cooling process is IBS. Therefore it is necessary to understand and simulate precisely how it affects the beam parameters for realistic beam distributions.

Using the reference of beam profile measurements in the AD we have generated input macroparticle distributions for beam tracking simulation studies of ELENA. For these simulations initial beam bi-Gaussian (core-tail) $\bar{\mathrm{p}}$ transverse distributions have been considered as an input for the electron cooling simulation of coasting beams using the code BETACOOL. Although replacing the real profile by a bi-Gaussian distribution is a simplification, it constitutes an important improvement compared to a simple Gaussian approximation to get a better understanding of the influence of a halo in the initial contribution.

Three different IBS models have been compared during the cooling process for the first cooling plateau of the ELENA cycle: the so-called (standard) Martini model [5], the simplified kinetic model [29] and a local model [30].

It has clearly been shown that the cooling simulation results depend strongly on the IBS model applied. Therefore, it is very important to select an adequate model depending on the accuracy level required for the beam evolution predictions. In a cooling process, where the beam can deviate quickly from the Gaussian profile, the use of a shape-independent model is appropriate. For instance, the use of a local model, although very demanding in terms of computing time, is useful to avoid unphysical results, such as beam core overcooling.

We are planning to complete this study performing a start-to-end simulation for the whole ELENA cycle. This will include realistic assumptions of initial particle distributions, based on real measurements, and also using beam-shape IBS independent models. Of course, following the usual procedure for these kind of studies, the validation of any computation model will be determined by comparison with measurements during the commissioning phase and future operation of the machine.

It is also important to mention that whilst done for the ELENA case, the conclusions from this paper are also well suited for other future low energy antiproton and ion machines, for example the Ultra-low energy Storage Ring (USR) [35] in the context of the future Facility for Low-energy Antiproton and Ion Research (FLAIR) at GSI [36].

Acknowledgments

We gratefully acknowledge A. V. Smirnov for providing us with the latest version of the code BETACOOL, and all our colleagues from the ELENA team at CERN for very fruitful discussions. Specially we would like to thank C. Carli for his continuous support to this study and very valuable suggestions and discussions.

This work is supported by the EU under Grant Agreement 624854 and the STFC Cockcroft Institute core Grant No. ST/G008248/1.

References

[1] S. Maury (editor), Design Study of the Antiproton Decelerator: AD, CERN/PS 96-43 (AR), 1996.

[2] V. Chohan (editor) et al., Extra Low Energy Antiproton ring (ELENA) and its Transfer Lines, Design Report, CERN-2014-002 (2014).

[3] G. Tranquile, A. Frassier, L. Joergensen, The ELENA electron cooler: parameter choice and expected performance, Proceedings of COOL2013, WEPPO16, Murren, Switzerland, 2013.

[4] J. Resta-Lopez et al., Simulation studies of the beam cooling process in presence of heating effects in the Extra Low ENergy Antiproton ring (ELENA), JINST **10** (2015) P05012.

[5] M. Martini, Intrabeam Scattering in the ACOL-AA Machines, CERN-PS-AA-84-9, 1984.

[6] A. Piwinski, Intra-Beam Scattering, Proceedings of the 9th International Conference on High Energy Accelerators, Stanford, CA, 1974, p. 405.

[7] J. Bjorken, S. Mtingwa, Intrabeam Scattering, Part. Accel. **13**, 115 (1983).

[8] A. Piwinski, Intra-Beam Scattering, CERN Report 92-01 (1992), p. 226.

[9] A. Sidorin et al., BETACOOL program for simulation of beam dynamics in storage rings, Nucl. Instrum. Methods Phys. Res. A **558** (2006) 325.

[10] http://mad.web.cern.ch/mad/.

[11] P. Belochitskii, ELENA Project Status, Proceedings of COOL2013, THPMIHA02, Murren, Switzerland, 2013.

[12] T. Eriksson, private communication.

[13] S. Duarte Pinto et al., GEM-based beam profile monitors for the antiproton decelerator, JINST **7** (2012) C03001.

[14] J. Spanggaard et al., GEM detectors for the transverse profile measurement of low energy antiprotons and high energy hadrons, Proceedings of IPAC2013, MOPWA036, Shanghai, China, 2013.

[15] J. F. Comblin, S. Hancock, J. L. Sanchez Alvarez, A pedestrian guide to online phase space tomography in the CERN PS complex, CERN-PS-RF-Note-2001-010, 2001.

[16] A. Chao (ed.) et al., Handbook of Accelerator Physics and Engineering, Second ed., World Scientific Publishing, Singapore, 2013, 378.

[17] A. I. Papash et al., Nonlinear and long-term beam dynamics in low energy storage rings, Phys. Rev. ST-AB **16** (2013) 060101.

[18] G. I. Budker, An effective method of damping particle oscillations in proton and antiproton storage rings, Atomnaya Energiya **22** (1967) 346.

[19] Ya. S. Debernev and A. N. Skrinsky, The effect of an accompanying magnetic field on electron cooling, Part. Accel. **8** (1978) 235.

[20] A. H. Sorensen and E. Bonderup, Electron cooling, Nucl. Instrum. Methods Phys. Res. **215** (1983) 27.

[21] I. N. Meshkov, Electron cooling –the first 30 years and thereafter, Nucl. Instrum. Methods Phys. Res. A **391** (1997) 1.

[22] V. V. Parkhomchuk, New insights in the theory of electron cooling, Nucl. Instrum. Methods Phys. Res. A **441** (2000) 9.

[23] A. V. Fedotov et al., Numerical study of the magnetized friction force, Phys. Rev. ST-AB **9** (2006) 074401.

[24] A. V. Fedotov et al., Experimental studies of magnetized friction force, Phys. Rev. E **73** (2006) 066503.

[25] A. V. Fedotov, IBS for Ion Distribution Under Electron Cooling, Proceedings of PAC05, Knoxville, Tennessee, USA, 2005.

[26] A. V. Fedotov, A. O. Sidorin, A. Smirnov, IBS for Non-Gaussian Distributions, BNL-94081-2010-CP (2010).

[27] A. Burov, Electron Cooling against IBS for High Energy Colliders, FERMILAB-TM-2213 (2003).

[28] G. Parzen, BNL Tech. Note C-AD/AP/150 (2004).

[29] P. Zenkevich, O. Boine-Frankenheim, A. Bolshakov, Nucl. Instrum. Methods Phys. Res. A **561** (2006) 284.

[30] A. Sidorin, Cooling simulations with the BETACOOL code, Proceedings of COOL2007, MOM2I04, Bad Kreuznach, Germany, 2007.

[31] BNL BETACOOL report, Dec. 2007: http://betacool.jinr.ru/reports.

[32] J. Resta-Lopez, J. R. Hunt and C. P. Welsch, Intra-beam scattering effects in ELENA, Proceedings of IPAC2016, WEAB3, Richmond, Virginia, USA, 2016.

[33] R. Keservan, private communication.

[34] C. Carli et al., Review of rest gas interaction at very low energies applied to the Extra Low Energy Antiproton Ring ELENA, Proceedings of IPAC2014, TUPRI028, Dresden, Germany, 2014.

[35] C. P. Welsch, Ultra-low energy storage ring at FLAIR, Hyperfine Interact. **213** (2012) 205.

[36] C. P. Welsch et al., FLAIR Project at GSI, AIP Conf. Proc. **821** (2006) 85.

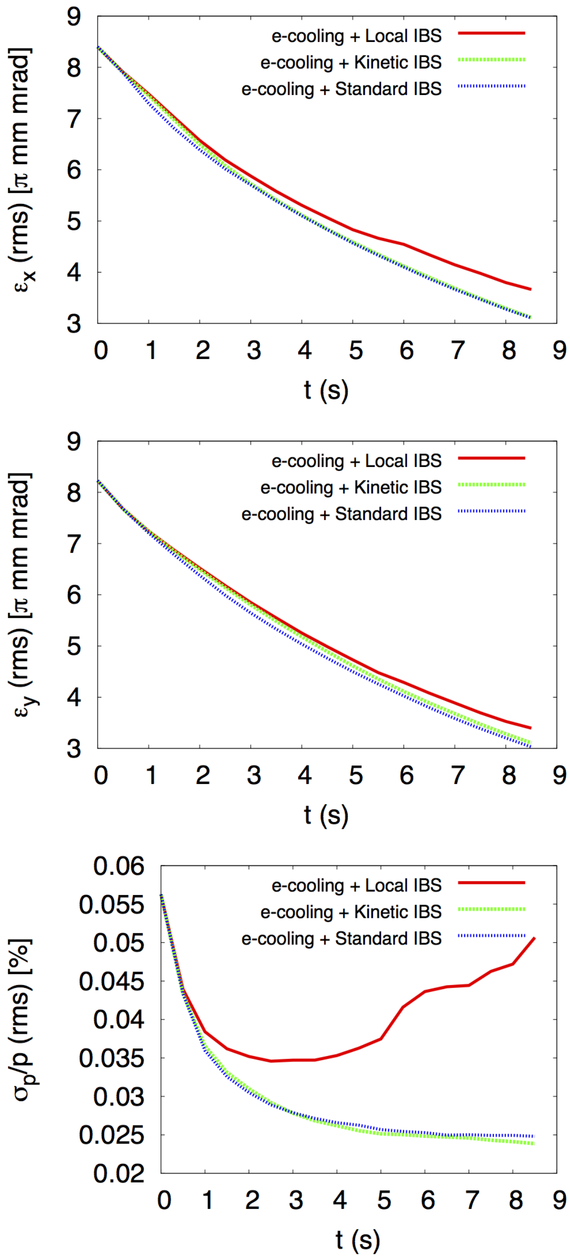

Figure 8: Beam parameter time evolution over the e-cooling process at 35 MeV/c momentum: rms horizontal (top) and vertical (middle) rms emittances, and relative rms momentum spread (bottom). The action of different IBS models is compared.

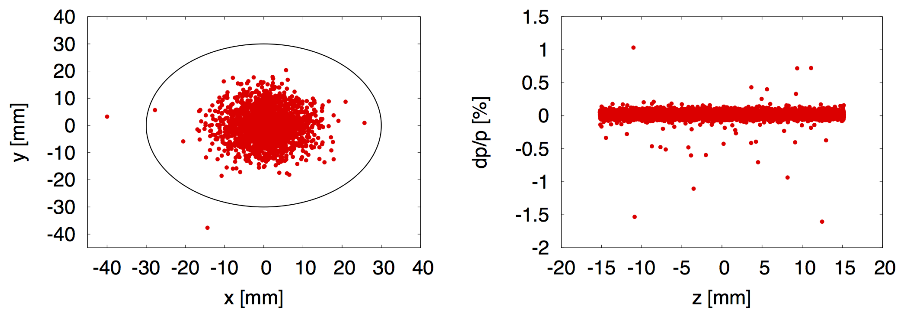

Figure 9: Transverse (left) and longitudinal (right) particle distribution after 8 s cooling at 35 MeV/c momentum for the case e-cooling + local IBS. The solid black circle represents the effective physical transverse aperture of the beampipe.

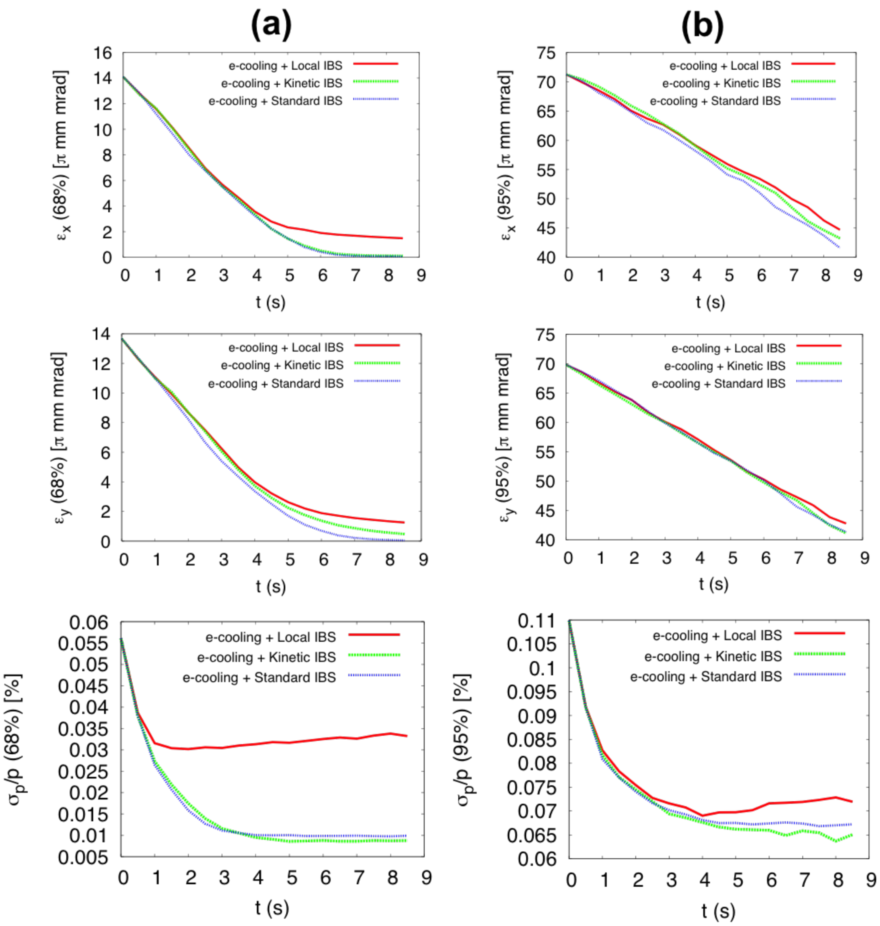

Figure 10: Transverse emittances and relative momentum spread for half beam widths containing 68% of the particles (a), and 95% of the particles (b).

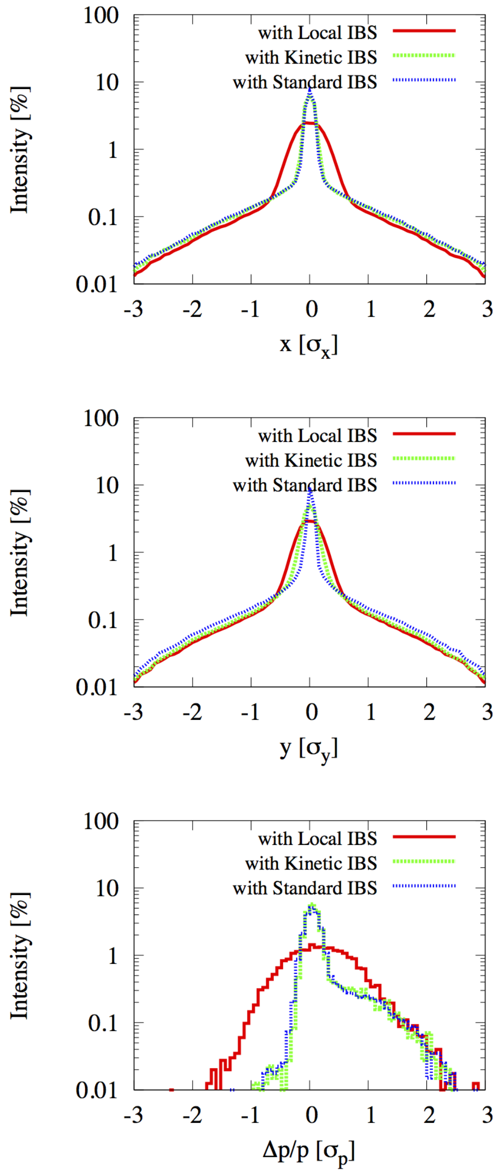

Figure 11: Horizontal (top), vertical (middle) and momentum spread (bottom) distributions after 8 s cooling at 35 MeV/c momentum, comparing the performance under the action of different IBS models. The horizontal axis is written in units of initial rms widths. The intensity is normalised over the corresponding initial rms parameter and the total number of macroparticles.